

A. ADDITIONAL QUANTITATIVE RESULTS

TABLE IV

HOLD-OUT TEST SET RESULTS FOR ALL MODELS. ‘#’ REFERS TO THE NUMBER OF RECORDINGS IN THE TEST SET WHERE THE SIGNAL WAS AVAILABLE. AVERAGE ACCURACY IN TERMS OF 5-, 4-, 3-, AND 2-CLASS SLEEP STAGING IS SHOWN HERE.

| Signal(s) | # | Accuracy [%] | | | |
|------------------------------|-----|----------------|----------------|------------|------------|
| | | W/N1/N2/N3/REM | W/N1-N2/N3/REM | W/NREM/REM | Wake/Sleep |
| All PSG electrodes | 497 | 85.9 | 89.8 | 93.4 | 96.4 |
| Left EEG electrodes | 500 | 85.5 | 89.5 | 93.3 | 96.4 |
| F3-M2 (EEG) | 500 | 85.6 | 89.5 | 93.1 | 96.2 |
| C3-M2 (EEG) | 500 | 85.3 | 89.4 | 93.2 | 96.2 |
| O1-M2 (EEG) | 500 | 83.4 | 87.9 | 92.6 | 96.1 |
| Recommended PSG electrodes | 497 | 86.3 | 90.2 | 93.6 | 96.5 |
| Right EEG electrodes | 500 | 85.8 | 89.8 | 93.3 | 96.5 |
| F4-M1 (EEG) | 500 | 85.5 | 89.4 | 93.0 | 96.1 |
| C4-M1 (EEG) | 500 | 85.5 | 89.6 | 93.2 | 96.3 |
| O2-M1 (EEG) | 500 | 83.8 | 88.2 | 92.7 | 96.2 |
| E2-M2 (EOG) | 497 | 85.0 | 89.2 | 93.2 | 96.2 |
| E1-M2 (EOG) | 500 | 84.3 | 88.8 | 92.9 | 95.9 |
| Chin1-Chin2 (EMG) | 500 | 74.9 | 80.9 | 88.1 | 92.7 |
| Chin2-Chin3 (EMG) | 500 | 74.9 | 80.9 | 88.0 | 92.6 |
| Chin1-Chin3 (EMG) | 500 | 74.5 | 80.6 | 87.8 | 92.5 |
| HSAT expanded | 434 | 79.0 | 84.3 | 90.8 | 94.4 |
| HSAT reduced | 434 | 78.3 | 83.6 | 90.2 | 94.1 |
| Nasal cannula | 434 | 76.5 | 81.9 | 89.0 | 93.4 |
| Finger PPG | 500 | 75.1 | 80.8 | 88.0 | 92.4 |
| Thoracic belt | 500 | 76.3 | 82.7 | 89.7 | 93.6 |
| HSAT reduced | 434 | 77.6 | 82.9 | 89.6 | 93.8 |
| Nasal cannula | 434 | 76.5 | 81.9 | 89.0 | 93.4 |
| IHR from finger PPG | 500 | 71.8 | 77.6 | 84.9 | 90.0 |
| HSAT expanded | 434 | 78.5 | 84.0 | 90.6 | 94.1 |
| HSAT reduced | 434 | 77.7 | 83.1 | 89.9 | 93.5 |
| thermistor | 434 | 72.9 | 79.2 | 87.0 | 91.6 |
| ECG | 500 | 76.9 | 82.2 | 89.1 | 93.2 |
| Thoracic belt | 500 | 76.3 | 82.7 | 89.7 | 93.6 |
| HSAT expanded | 66 | 78.2 | 83.5 | 90.5 | 93.7 |
| HSAT reduced | 66 | 76.4 | 81.2 | 88.5 | 92.1 |
| PAP flow | 66 | 69.5 | 74.4 | 83.1 | 87.8 |
| Finger PPG | 500 | 75.1 | 80.8 | 88.0 | 92.4 |
| Thoracic belt | 500 | 76.3 | 82.7 | 89.7 | 93.6 |
| HSAT reduced | 65 | 74.9 | 80.1 | 87.0 | 92.0 |
| IBR from PAP flow | 65 | 69.2 | 74.8 | 83.0 | 89.3 |
| IHR from finger PPG | 500 | 71.8 | 77.6 | 84.9 | 90.0 |
| Left Leg and SCM | 33 | 71.0 | 77.0 | 85.1 | 90.7 |
| Left Leg (EMG) | 500 | 66.9 | 72.2 | 81.2 | 88.5 |
| Left SCM (EMG) | 33 | 66.2 | 72.4 | 80.5 | 89.5 |
| Right Leg and SCM | 33 | 70.3 | 76.3 | 84.4 | 90.2 |
| Right Leg (EMG) | 500 | 66.7 | 72.0 | 80.8 | 88.2 |
| Right SCM (EMG) | 33 | 67.0 | 73.1 | 81.7 | 89.7 |
| Left Leg and FDS | 60 | 67.4 | 72.8 | 81.8 | 88.7 |
| Left Leg (EMG) | 500 | 66.9 | 72.2 | 81.2 | 88.5 |
| Left FDS (EMG) | 60 | 63.7 | 69.5 | 78.8 | 88.2 |
| Right Leg and FDS | 60 | 68.0 | 73.1 | 82.0 | 88.6 |
| Right Leg (EMG) | 500 | 66.7 | 72.0 | 80.8 | 88.2 |
| Right FDS (EMG) | 60 | 63.2 | 69.1 | 78.2 | 87.9 |
| Abdominal belt | 500 | 76.4 | 83.0 | 89.9 | 93.6 |
| Snore microphone | 500 | 72.1 | 78.0 | 85.9 | 91.9 |
| IHR from ECG | 500 | 70.1 | 75.8 | 83.8 | 89.1 |
| IBR from RIP thorax | 500 | 70.0 | 76.1 | 83.9 | 89.7 |
| IBR from RIP abdomen | 500 | 69.9 | 76.1 | 84.0 | 89.7 |
| SpO2 | 500 | 68.7 | 74.7 | 82.8 | 89.1 |
| IBR from nasal cannula | 434 | 66.9 | 73.3 | 81.5 | 87.5 |
| IBR from Thermistor | 434 | 65.4 | 72.0 | 80.8 | 87.4 |
| Suprasternal notch | 72 | 63.1 | 69.5 | 78.4 | 86.0 |
| IBR from esophageal pressure | 24 | 59.0 | 67.9 | 76.7 | 83.2 |
| IBR from Suprasternal notch | 72 | 58.5 | 65.3 | 74.5 | 82.2 |
| Esophageal pressure | 24 | 55.5 | 62.1 | 72.5 | 80.7 |

TABLE V

HOLD-OUT TEST SET RESULTS FOR ALL MODELS. ‘#’ REFERS TO THE NUMBER OF RECORDINGS IN THE HOLD-OUT TEST SET WHERE THE SIGNAL WAS AVAILABLE. AVERAGE COHEN’S KAPPA IN TERMS OF 5-,4-,3-, AND 2-CLASS SLEEP STAGING IS SHOWN HERE.

| Signal(s) | # | Cohen’s Kappa | | | |
|------------------------------|-----|----------------|----------------|------------|------------|
| | | W/N1/N2/N3/REM | W/N1-N2/N3/REM | W/NREM/REM | Wake/Sleep |
| All PSG electrodes | 497 | 0.793 | 0.826 | 0.853 | 0.858 |
| Left EEG electrodes | 500 | 0.789 | 0.822 | 0.850 | 0.863 |
| F3-M2 (EEG) | 500 | 0.791 | 0.823 | 0.846 | 0.855 |
| C3-M2 (EEG) | 500 | 0.787 | 0.821 | 0.848 | 0.857 |
| O1-M2 (EEG) | 500 | 0.760 | 0.795 | 0.835 | 0.850 |
| Recommended PSG electrodes | 497 | 0.799 | 0.832 | 0.856 | 0.864 |
| Right EEG electrodes | 500 | 0.794 | 0.827 | 0.851 | 0.863 |
| F4-M1 (EEG) | 500 | 0.790 | 0.822 | 0.844 | 0.850 |
| C4-M1 (EEG) | 500 | 0.791 | 0.824 | 0.848 | 0.857 |
| O2-M1 (EEG) | 500 | 0.764 | 0.800 | 0.837 | 0.851 |
| E2-M2 (EOG) | 497 | 0.784 | 0.820 | 0.850 | 0.858 |
| E1-M2 (EOG) | 500 | 0.776 | 0.815 | 0.845 | 0.852 |
| Chin1-Chin2 (EMG) | 500 | 0.630 | 0.677 | 0.737 | 0.716 |
| Chin2-Chin3 (EMG) | 500 | 0.631 | 0.678 | 0.735 | 0.716 |
| Chin1-Chin3 (EMG) | 500 | 0.624 | 0.672 | 0.731 | 0.709 |
| HSAT expanded | 434 | 0.697 | 0.740 | 0.801 | 0.793 |
| HSAT reduced | 434 | 0.686 | 0.731 | 0.791 | 0.783 |
| Nasal cannula | 434 | 0.661 | 0.705 | 0.767 | 0.762 |
| Finger PPG | 500 | 0.640 | 0.685 | 0.746 | 0.735 |
| Thoracic belt | 500 | 0.657 | 0.708 | 0.775 | 0.765 |
| HSAT reduced | 434 | 0.676 | 0.719 | 0.777 | 0.774 |
| Nasal cannula | 434 | 0.661 | 0.705 | 0.767 | 0.762 |
| IHR from finger PPG | 500 | 0.597 | 0.637 | 0.693 | 0.688 |
| HSAT expanded | 434 | 0.687 | 0.733 | 0.797 | 0.787 |
| HSAT reduced | 434 | 0.674 | 0.720 | 0.785 | 0.774 |
| thermistor | 434 | 0.603 | 0.650 | 0.717 | 0.702 |
| ECG | 500 | 0.669 | 0.711 | 0.773 | 0.772 |
| Thoracic belt | 500 | 0.657 | 0.708 | 0.775 | 0.765 |
| HSAT expanded | 66 | 0.678 | 0.722 | 0.797 | 0.778 |
| HSAT reduced | 66 | 0.652 | 0.690 | 0.759 | 0.735 |
| PAP flow | 66 | 0.562 | 0.594 | 0.661 | 0.634 |
| Finger PPG | 500 | 0.640 | 0.685 | 0.746 | 0.735 |
| Thoracic belt | 500 | 0.657 | 0.708 | 0.775 | 0.765 |
| HSAT reduced | 65 | 0.626 | 0.666 | 0.719 | 0.699 |
| IBR from PAP flow | 65 | 0.538 | 0.580 | 0.634 | 0.579 |
| IHR from finger PPG | 500 | 0.597 | 0.637 | 0.693 | 0.688 |
| Left Leg and SCM | 33 | 0.575 | 0.624 | 0.699 | 0.716 |
| Left Leg (EMG) | 500 | 0.526 | 0.558 | 0.621 | 0.632 |
| Left SCM (EMG) | 33 | 0.502 | 0.546 | 0.594 | 0.681 |
| Right Leg and SCM | 33 | 0.565 | 0.613 | 0.689 | 0.700 |
| Right Leg (EMG) | 500 | 0.523 | 0.556 | 0.616 | 0.629 |
| Right SCM (EMG) | 33 | 0.517 | 0.561 | 0.627 | 0.679 |
| Left Leg and FDS | 60 | 0.532 | 0.566 | 0.633 | 0.647 |
| Left Leg (EMG) | 500 | 0.526 | 0.558 | 0.621 | 0.632 |
| Left FDS (EMG) | 60 | 0.482 | 0.510 | 0.555 | 0.615 |
| Right Leg and FDS | 60 | 0.540 | 0.569 | 0.639 | 0.647 |
| Right Leg (EMG) | 500 | 0.523 | 0.556 | 0.616 | 0.629 |
| Right FDS (EMG) | 60 | 0.476 | 0.503 | 0.544 | 0.609 |
| Abdominal belt | 500 | 0.661 | 0.715 | 0.779 | 0.770 |
| Snore microphone | 500 | 0.597 | 0.639 | 0.692 | 0.714 |
| IHR from ECG | 500 | 0.571 | 0.609 | 0.670 | 0.659 |
| IBR from RIP thorax | 500 | 0.564 | 0.611 | 0.662 | 0.626 |
| IBR from RIP abdomen | 500 | 0.563 | 0.612 | 0.664 | 0.625 |
| SpO2 | 500 | 0.542 | 0.589 | 0.642 | 0.624 |
| IBR from nasal cannula | 434 | 0.521 | 0.568 | 0.616 | 0.563 |
| IBR from Thermistor | 434 | 0.497 | 0.545 | 0.597 | 0.536 |
| Suprasternal notch | 72 | 0.464 | 0.499 | 0.553 | 0.573 |
| IBR from esophageal pressure | 24 | 0.419 | 0.473 | 0.523 | 0.474 |
| IBR from Suprasternal notch | 72 | 0.394 | 0.433 | 0.473 | 0.431 |
| Esophageal pressure | 24 | 0.373 | 0.410 | 0.466 | 0.483 |

TABLE VI

HOLD-OUT TEST SET RESULTS FOR ALL MODELS. ‘#’ REFERS TO THE NUMBER OF RECORDINGS IN THE HOLD-OUT TEST SET WHERE THE SIGNAL WAS AVAILABLE. AVERAGE F1-SCORES PER SLEEP STAGE ARE SHOWN HERE.

| Signal(s) | # | F1 scores | | | | |
|------------------------------|-----|-----------|-------|-------|-------|-------|
| | | Wake | N1 | N2 | N3 | REM |
| All PSG electrodes | 497 | 0.885 | 0.588 | 0.881 | 0.834 | 0.882 |
| Left EEG electrodes | 500 | 0.888 | 0.599 | 0.876 | 0.821 | 0.871 |
| F3-M2 (EEG) | 500 | 0.882 | 0.593 | 0.878 | 0.833 | 0.869 |
| C3-M2 (EEG) | 500 | 0.883 | 0.596 | 0.874 | 0.826 | 0.872 |
| O1-M2 (EEG) | 500 | 0.878 | 0.574 | 0.857 | 0.767 | 0.857 |
| Recommended PSG electrodes | 497 | 0.890 | 0.598 | 0.883 | 0.845 | 0.881 |
| Right EEG electrodes | 500 | 0.886 | 0.599 | 0.879 | 0.833 | 0.871 |
| F4-M1 (EEG) | 500 | 0.876 | 0.591 | 0.879 | 0.834 | 0.868 |
| C4-M1 (EEG) | 500 | 0.882 | 0.598 | 0.877 | 0.828 | 0.872 |
| O2-M1 (EEG) | 500 | 0.878 | 0.572 | 0.859 | 0.787 | 0.858 |
| E2-M2 (EOG) | 497 | 0.887 | 0.577 | 0.865 | 0.828 | 0.876 |
| E1-M2 (EOG) | 500 | 0.881 | 0.582 | 0.855 | 0.821 | 0.874 |
| Chin1-Chin2 (EMG) | 500 | 0.766 | 0.352 | 0.778 | 0.677 | 0.813 |
| Chin2-Chin3 (EMG) | 500 | 0.767 | 0.353 | 0.778 | 0.683 | 0.810 |
| Chin1-Chin3 (EMG) | 500 | 0.760 | 0.342 | 0.775 | 0.677 | 0.807 |
| HSAT expanded | 434 | 0.833 | 0.434 | 0.811 | 0.724 | 0.845 |
| HSAT reduced | 434 | 0.824 | 0.393 | 0.804 | 0.718 | 0.832 |
| Nasal cannula | 434 | 0.806 | 0.375 | 0.787 | 0.702 | 0.811 |
| Finger PPG | 500 | 0.787 | 0.366 | 0.775 | 0.689 | 0.798 |
| Thoracic belt | 500 | 0.813 | 0.433 | 0.783 | 0.689 | 0.828 |
| HSAT reduced | 434 | 0.818 | 0.398 | 0.799 | 0.712 | 0.819 |
| Nasal cannula | 434 | 0.806 | 0.375 | 0.787 | 0.702 | 0.811 |
| IHR from finger PPG | 500 | 0.755 | 0.351 | 0.744 | 0.665 | 0.757 |
| HSAT expanded | 434 | 0.832 | 0.429 | 0.807 | 0.700 | 0.844 |
| HSAT reduced | 434 | 0.821 | 0.386 | 0.800 | 0.694 | 0.833 |
| thermistor | 434 | 0.759 | 0.331 | 0.762 | 0.640 | 0.774 |
| ECG | 500 | 0.821 | 0.399 | 0.786 | 0.699 | 0.829 |
| Thoracic belt | 500 | 0.813 | 0.433 | 0.783 | 0.689 | 0.828 |
| HSAT expanded | 66 | 0.820 | 0.373 | 0.814 | 0.669 | 0.853 |
| HSAT reduced | 66 | 0.788 | 0.320 | 0.798 | 0.670 | 0.834 |
| PAP flow | 66 | 0.709 | 0.239 | 0.733 | 0.591 | 0.784 |
| Finger PPG | 500 | 0.787 | 0.366 | 0.775 | 0.689 | 0.798 |
| Thoracic belt | 500 | 0.813 | 0.433 | 0.783 | 0.689 | 0.828 |
| HSAT reduced | 65 | 0.748 | 0.267 | 0.793 | 0.662 | 0.798 |
| IBR from PAP flow | 65 | 0.641 | 0.155 | 0.747 | 0.626 | 0.742 |
| IHR from finger PPG | 500 | 0.755 | 0.351 | 0.744 | 0.665 | 0.757 |
| Left Leg and SCM | 33 | 0.784 | 0.239 | 0.721 | 0.595 | 0.727 |
| Left Leg (EMG) | 500 | 0.709 | 0.226 | 0.698 | 0.598 | 0.689 |
| Left SCM (EMG) | 33 | 0.757 | 0.237 | 0.668 | 0.574 | 0.614 |
| Right Leg and SCM | 33 | 0.774 | 0.234 | 0.713 | 0.585 | 0.723 |
| Right Leg (EMG) | 500 | 0.705 | 0.220 | 0.696 | 0.597 | 0.680 |
| Right SCM (EMG) | 33 | 0.754 | 0.232 | 0.673 | 0.543 | 0.644 |
| Left Leg and FDS | 60 | 0.727 | 0.235 | 0.698 | 0.614 | 0.712 |
| Left Leg (EMG) | 500 | 0.709 | 0.226 | 0.698 | 0.598 | 0.689 |
| Left FDS (EMG) | 60 | 0.696 | 0.257 | 0.672 | 0.620 | 0.578 |
| Right Leg and FDS | 60 | 0.727 | 0.242 | 0.706 | 0.604 | 0.714 |
| Right Leg (EMG) | 500 | 0.705 | 0.220 | 0.696 | 0.597 | 0.680 |
| Right FDS (EMG) | 60 | 0.693 | 0.248 | 0.663 | 0.617 | 0.580 |
| Abdominal belt | 500 | 0.816 | 0.442 | 0.781 | 0.694 | 0.831 |
| Snore microphone | 500 | 0.771 | 0.362 | 0.749 | 0.668 | 0.729 |
| IHR from ECG | 500 | 0.732 | 0.346 | 0.729 | 0.637 | 0.740 |
| IBR from RIP thorax | 500 | 0.691 | 0.199 | 0.737 | 0.666 | 0.736 |
| IBR from RIP abdomen | 500 | 0.688 | 0.199 | 0.737 | 0.664 | 0.738 |
| SpO2 | 500 | 0.697 | 0.181 | 0.722 | 0.634 | 0.712 |
| IBR from nasal cannula | 434 | 0.639 | 0.179 | 0.712 | 0.651 | 0.709 |
| IBR from Thermistor | 434 | 0.610 | 0.157 | 0.701 | 0.610 | 0.698 |
| Suprasternal notch | 72 | 0.671 | 0.232 | 0.662 | 0.561 | 0.596 |
| IBR from esophageal pressure | 24 | 0.568 | 0.129 | 0.657 | 0.579 | 0.607 |
| IBR from Suprasternal notch | 72 | 0.541 | 0.112 | 0.639 | 0.566 | 0.587 |
| Esophageal pressure | 24 | 0.614 | 0.117 | 0.569 | 0.522 | 0.529 |

B. ADDITIONAL QUALITATIVE RESULTS

We here show a qualitative example for each of the signal(s) as shown in tables VI and IV. We show the most typical example for each, defined as the recording where it achieved median performance in terms of accuracy.

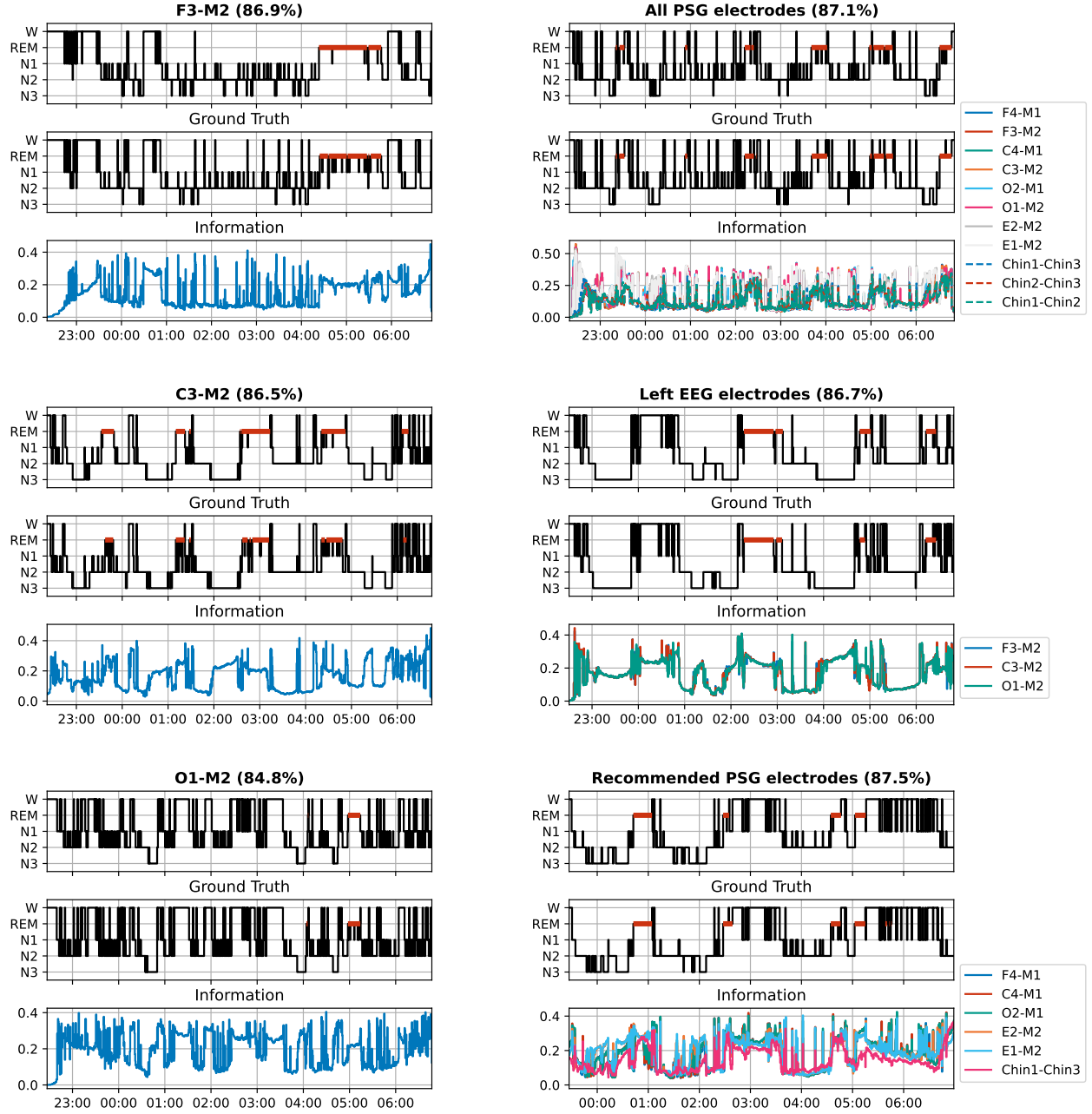


Fig. 9. Some additional qualitative examples.

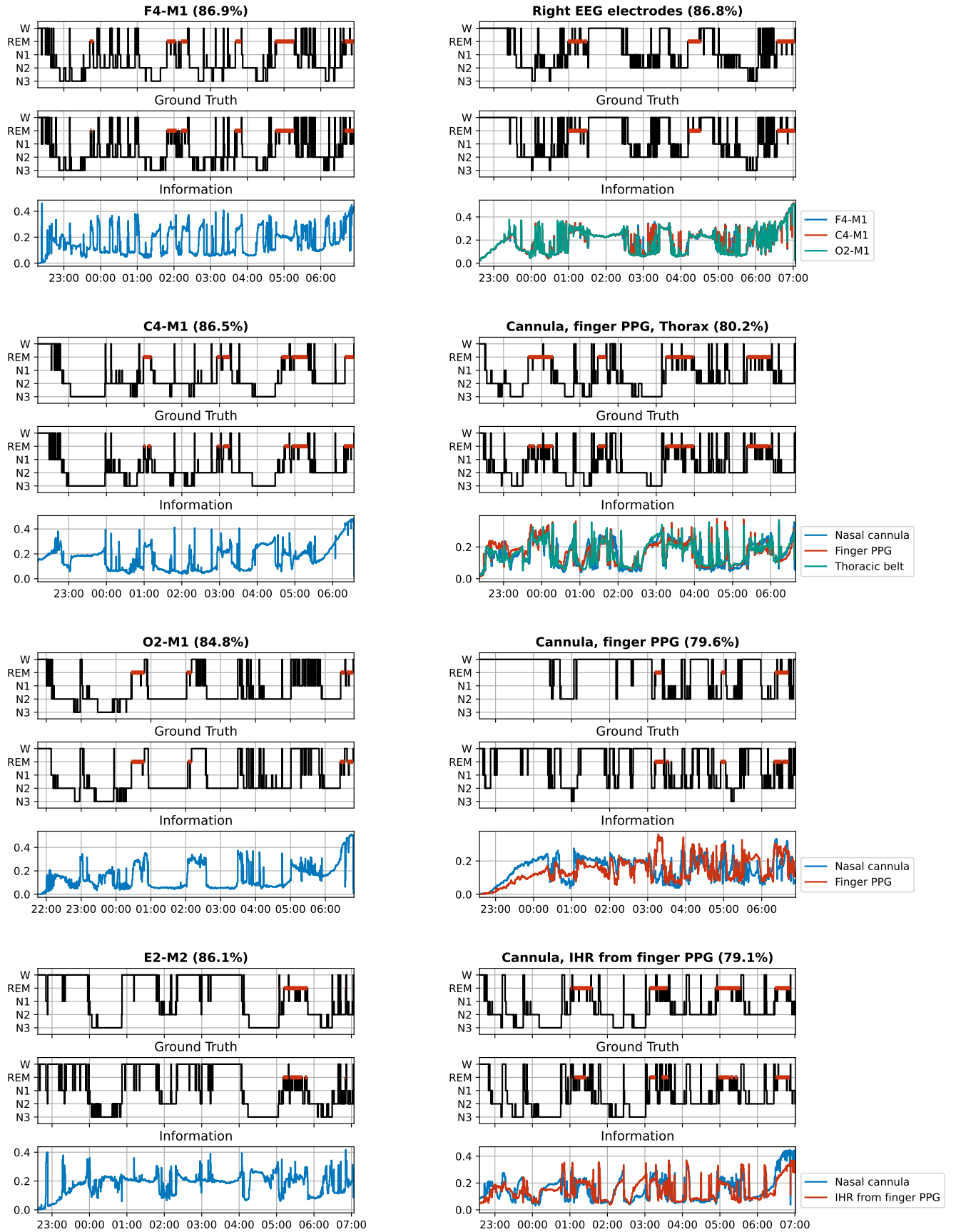


Fig. 10. Some additional qualitative examples.

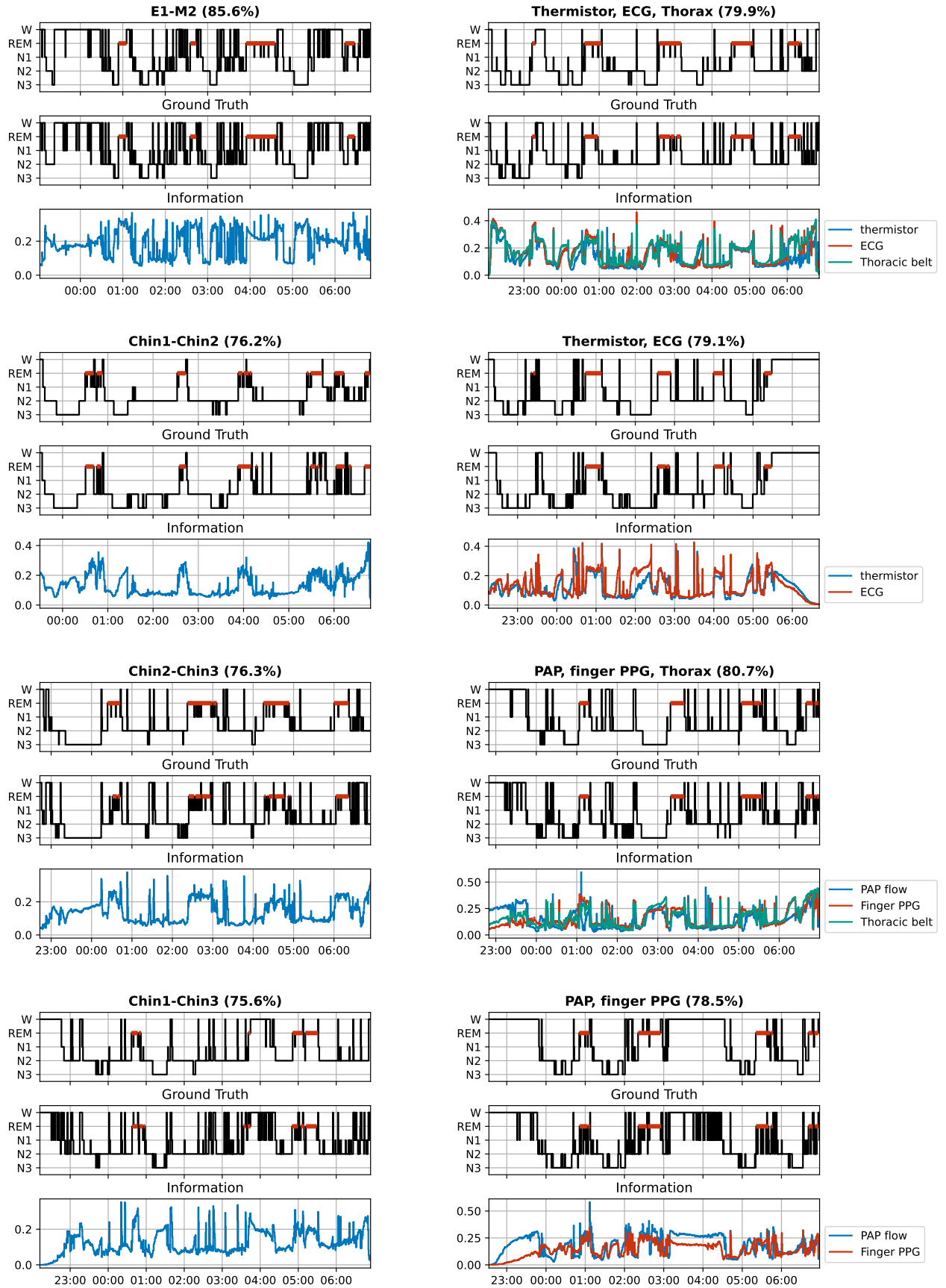


Fig. 11. Some additional qualitative examples.

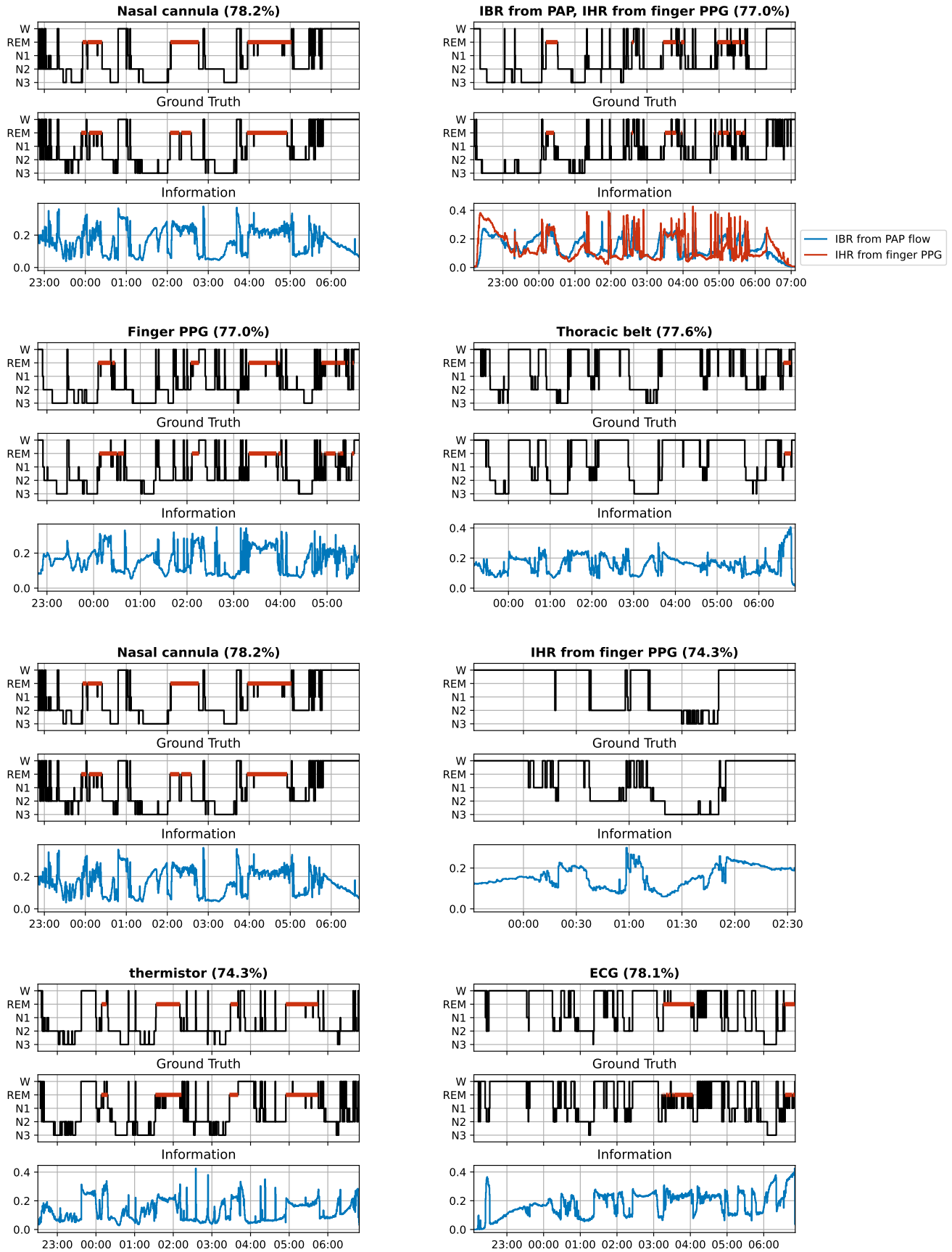


Fig. 12. Some additional qualitative examples.

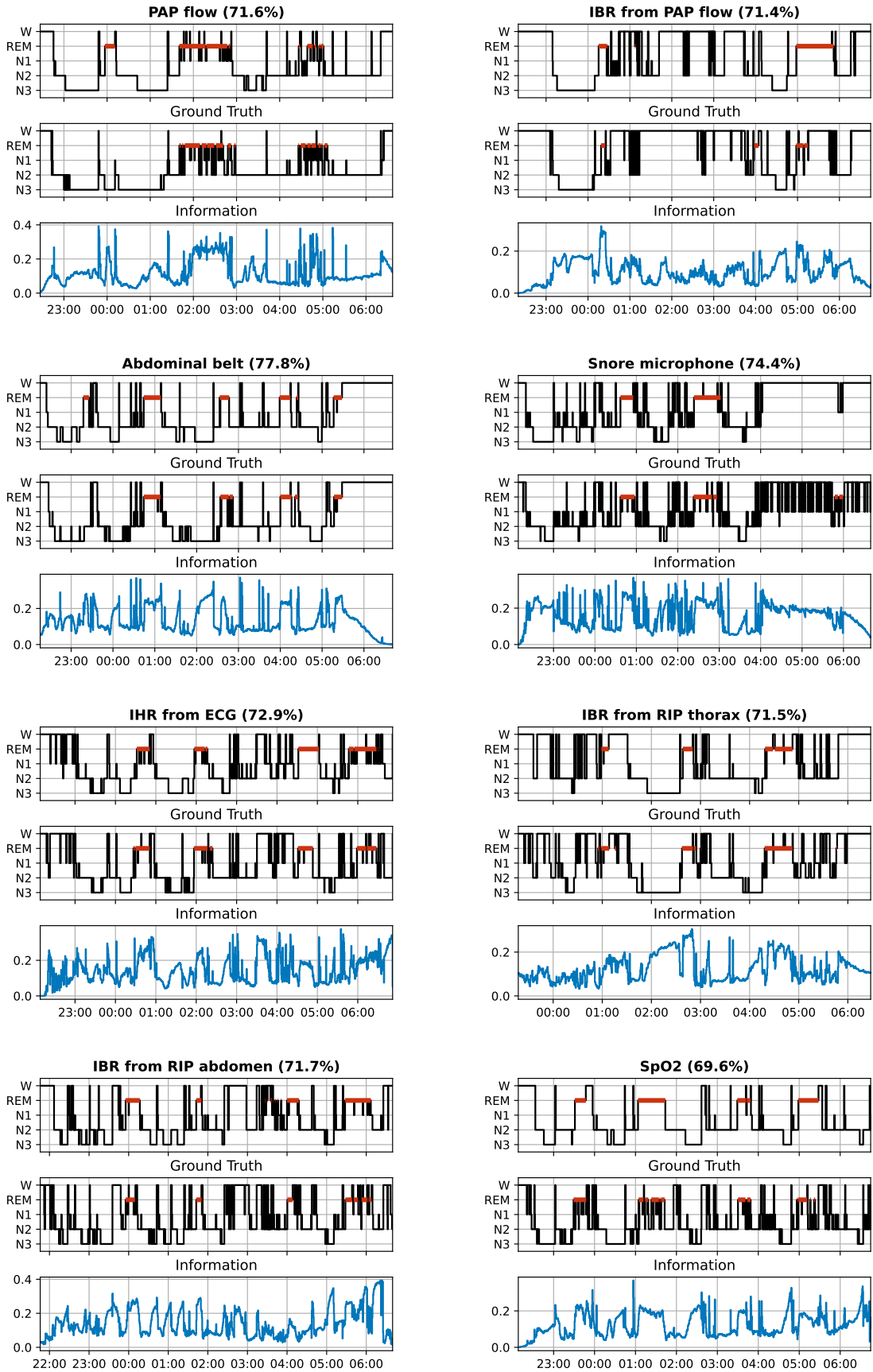


Fig. 13. Some additional qualitative examples.

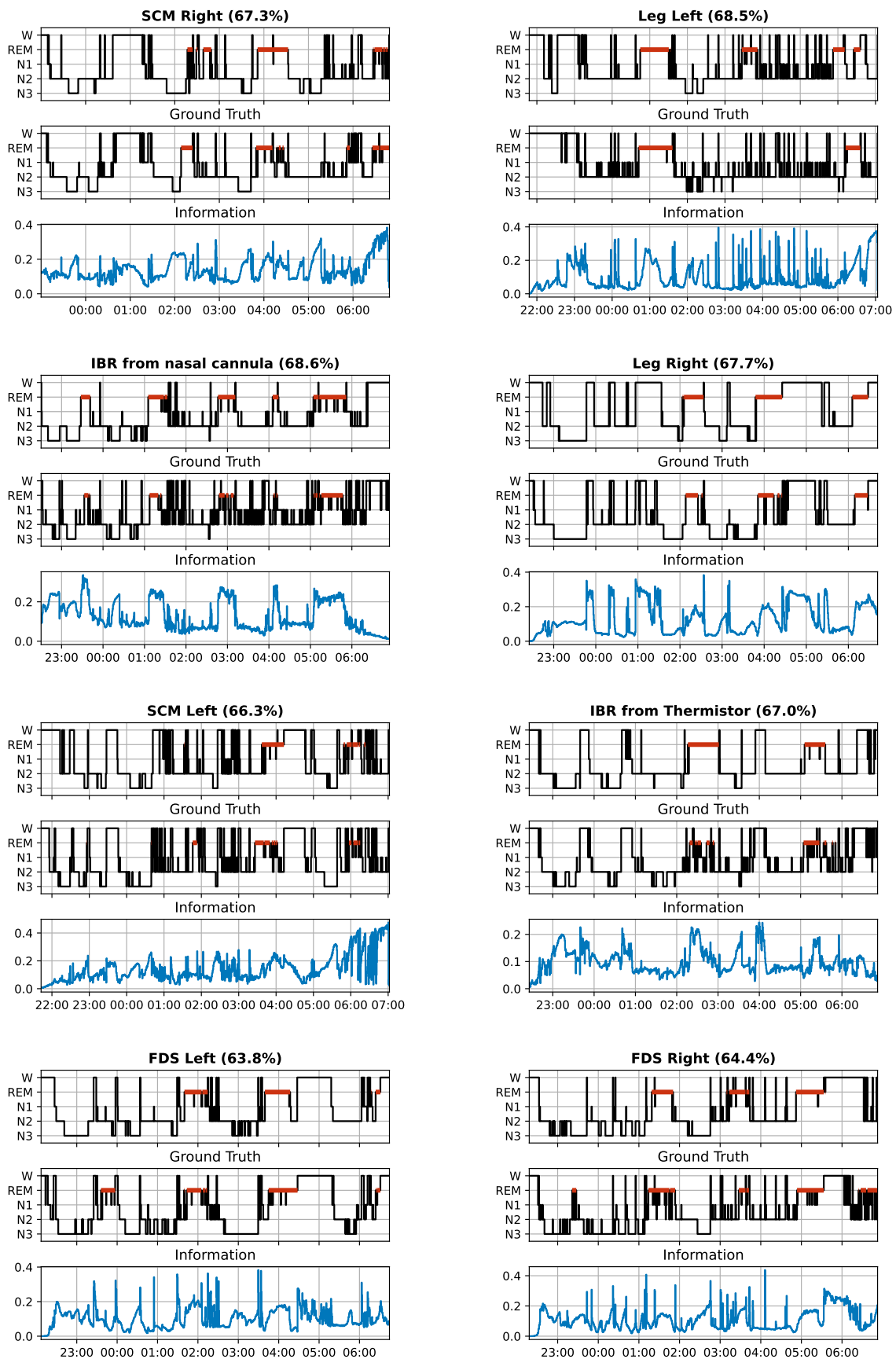


Fig. 14. Some additional qualitative examples.

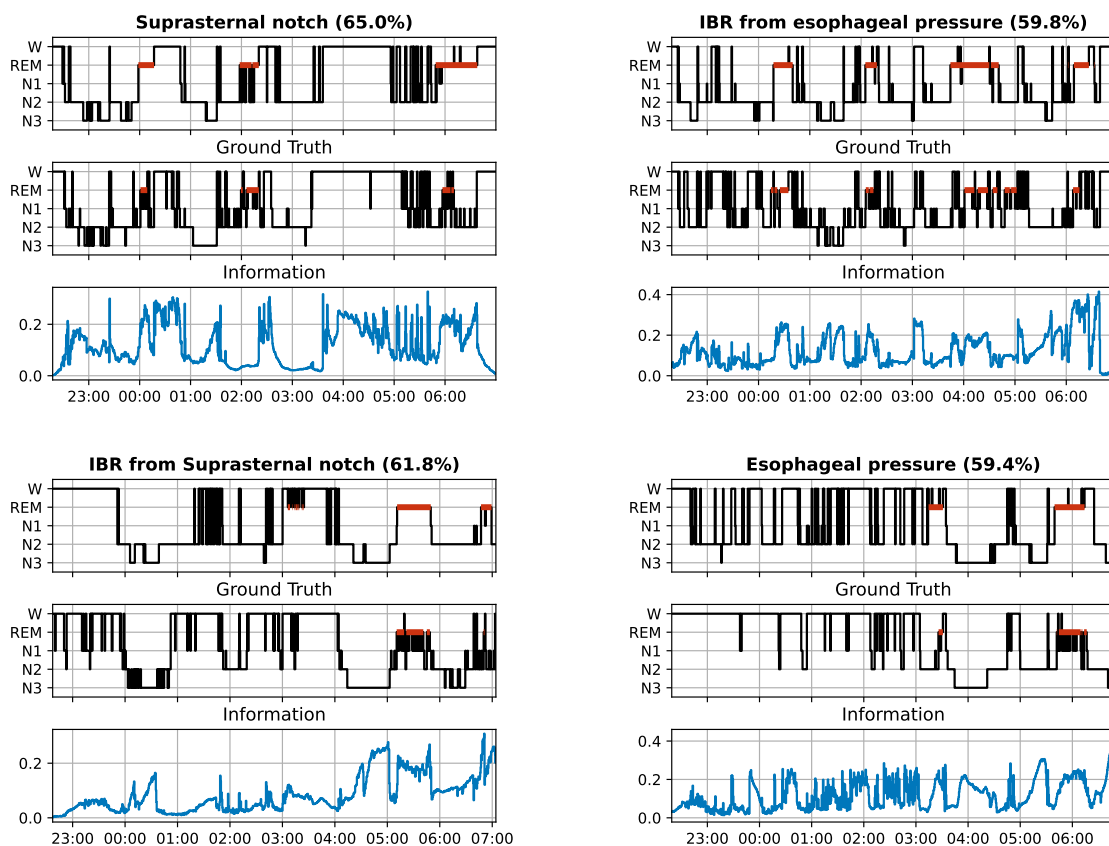


Fig. 15. Some additional qualitative examples.

C. SAMPLES FROM THE PRIOR

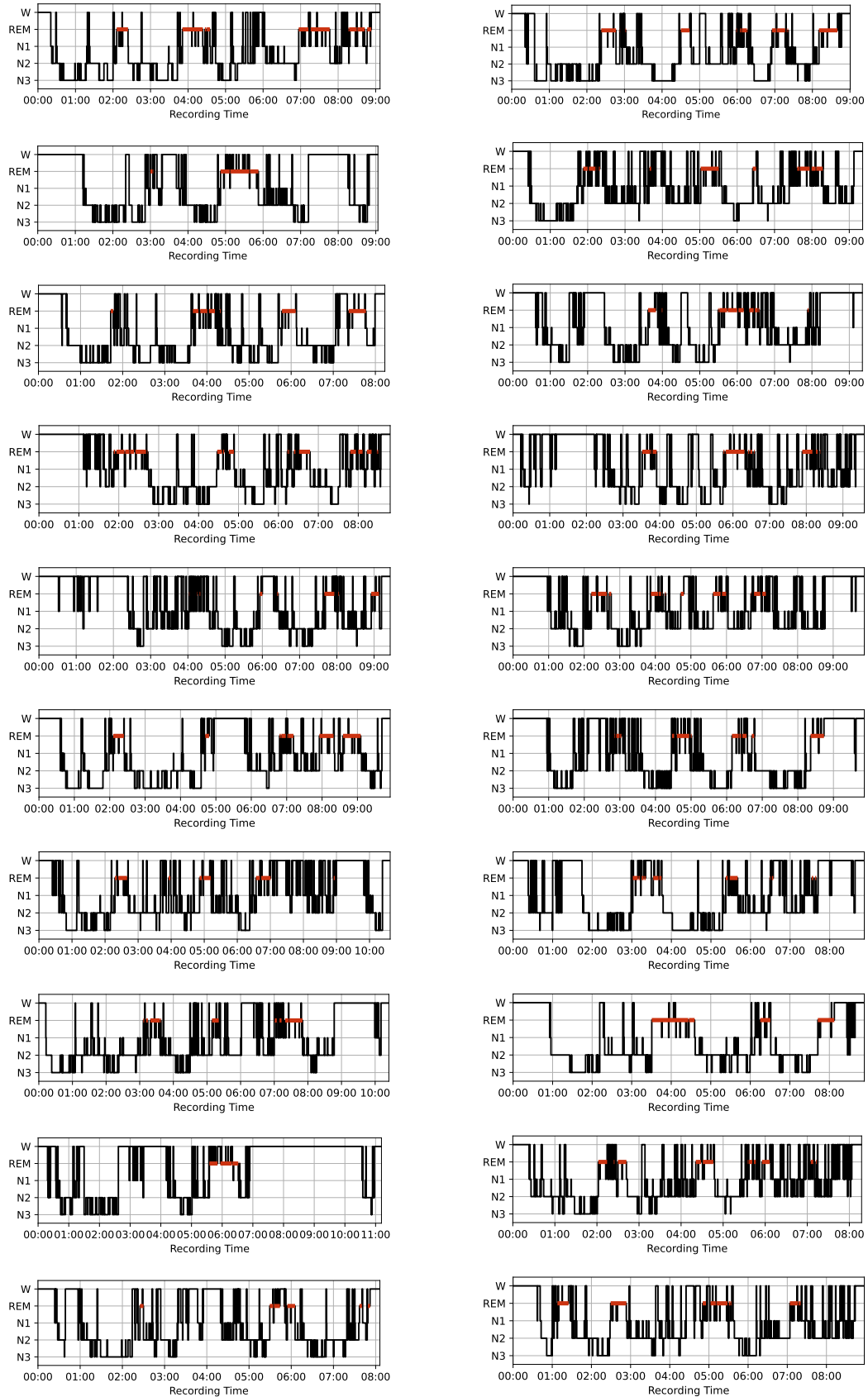


Fig. 16. We here show samples taken from the global prior score network (without the use of any measurement data).

D. INFORMATION GAIN VS PERFORMANCE

We here show the same experiment as shown in Fig.7 from the manuscript, but now for Cohen's kappa instead of accuracy.

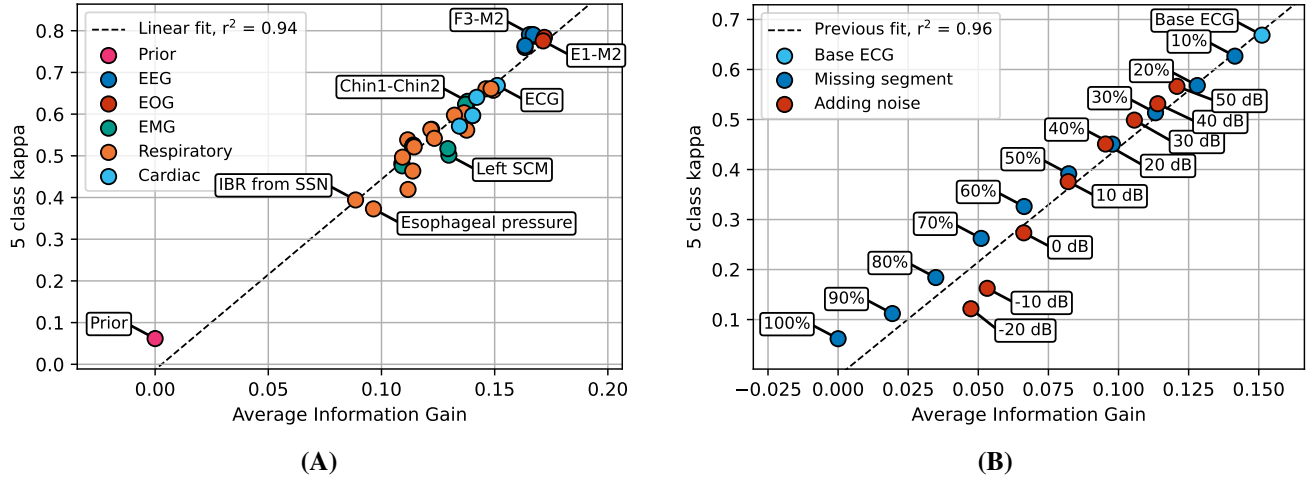


Fig. 17. Quantitative results for information gain. **(A)** The average information gain per sensor over all test recordings shows a clear linear correlation with respect to Cohen's kappa. **(B)** Reducing the usefulness of the ECG signal by removing segments or adding noise reduces down-stream accuracy and information gain. The linear relationship as fitted on the data from (A) still provides a good fit here.

E. INDIVIDUAL DIAGNOSES AND THEIR CLUSTERS

TABLE VII: Specific diagnoses and how they were clustered. Subjects could have multiple sleep disorders within the same cluster, e.g., a pediatric obstructive sleep apnea diagnosis and an adult obstructive sleep apnea diagnosis.

| Diagnosis | # | Cluster | # |
|---|------|--|------|
| Chronic insomnia disorder | 217 | Insomnia disorders | 613 |
| Psychophysiological insomnia | 206 | | |
| Idiopathic insomnia | 11 | | |
| Paradoxical insomnia | 23 | | |
| Inadequate sleep hygiene | 55 | | |
| Behavioral insomnia of childhood | 0 | | |
| Insomnia due to (another) mental disorder | 69 | | |
| Insomnia due to (a) medical condition | 86 | | |
| Other insomnia disorder | 31 | | |
| Obstructive sleep apnea, adult | 1037 | Obstructive Sleep Apnea | 1037 |
| Obstructive sleep apnea, pediatric | 4 | | |
| Central sleep apnea with Cheyne-Stokes breathing | 19 | Central Sleep Apnea | 42 |
| Central sleep apnea due to a medical disorder without Cheyne-Stokes breathing | 9 | | |
| Central sleep apnea due to a medication or substance | 3 | | |
| Primary central sleep apnea | 11 | | |
| Treatment emergent central sleep apnea | 6 | Treatment emergent central sleep apnea | 6 |
| Obesity hypoventilation syndrome | 1 | Hypoventilation | 8 |
| Idiopathic central alveolar hypoventilation | 1 | | |
| Sleep related hypoventilation due to a medication or substance | 1 | | |
| Sleep related hypoventilation due to a medical disorder | 0 | | |
| Sleep related hypoxemia disorder | 5 | | |
| Narcolepsy type 1 | 25 | Narcolepsy | 31 |
| Narcolepsy type 1 due to a medical condition | 1 | | |
| Narcolepsy type 2 | 5 | | |
| Narcolepsy type 2 due to a medical condition | 1 | | |
| Idiopathic hypersomnia | 8 | Other Hypersomnolence Disorders | 54 |
| Idiopathic hypersomnia with normal sleep time | 14 | | |
| Idiopathic hypersomnia with long sleep time | 8 | | |
| Kleine-Levin syndrome | 1 | | |
| Hypersomnia due to a medical disorder | 11 | | |
| Hypersomnia secondary to Parkinson disease | 4 | | |
| Residual hypersomnia in OSA patients with adequately treated OSA | 2 | | |
| Hypersomnia associated with a psychiatric disorder | 7 | | |
| Hypersomnia associated with mood disorder | 1 | | |
| Hypersomnia associated with a conversion disorder or somatic symptom disorder | 1 | | |
| Insufficient sleep syndrome | 66 | Insufficient sleep syndrome | 66 |

TABLE VII: Specific diagnoses and how they were clustered. Subjects could have multiple sleep disorders within the same cluster, e.g., a pediatric obstructive sleep apnea diagnosis and an adult obstructive sleep apnea diagnosis.

| Diagnosis | # | Cluster | # |
|--|-----|---|-----|
| Delayed sleep-wake phase disorder | 33 | Circadian rhythm disorders | 46 |
| Advanced sleep-wake phase disorder | 2 | | |
| Irregular sleep-wake rhythm disorder | 1 | | |
| Shift work disorder | 9 | | |
| Circadian sleep-wake disorder NOS | 1 | | |
| Confusional arousals | 74 | NREM parasomnias | 115 |
| Sleepwalking | 48 | | |
| Sleep terrors | 24 | | |
| Sleep related abnormal sexual behaviors | 2 | | |
| Sleep related eating disorder | 1 | | |
| REM sleep behavior disorder | 122 | RBD | 122 |
| Recurrent isolated sleep paralysis | 11 | REM parasomnias other than RBD | 55 |
| Nightmare disorder | 39 | | |
| Sleep related hallucinations | 12 | | |
| Parasomnia overlap disorder | 7 | Other parasomnias | 45 |
| Exploding head syndrome | 1 | | |
| Sleep enuresis | 2 | | |
| Parasomnia due to a medical disorder | 4 | | |
| Parasomnia, unspecified | 31 | | |
| Restless legs syndrome | 185 | RLS/PLMD | 268 |
| Periodic limb movement disorder | 114 | | |
| Sleep related leg cramps | 2 | Other movement disorders | 58 |
| Sleep related bruxism | 27 | | |
| Sleep related rhythmic movement disorder | 5 | | |
| Proprio-spinal myoclonus at sleep onset | 2 | | |
| Sleep related movement disorder, unspecified | 18 | | |
| Sleep starts (hypnic jerks) | 5 | | |
| Other sleep disorder | 5 | Other | 16 |
| Sleep related epilepsy | 2 | | |
| Sleep related headache | 1 | | |
| Sleep related laryngospasm | 4 | | |
| Sleep related gastroesophageal reflux | 3 | | |
| Sleep disorder due to sedative, hypnotic or anxiolytic | 1 | | |
| No primary sleep diagnosis | 45 | No primary sleep diagnosis and/or normal variants | 99 |
| Short sleeper | 2 | | |
| Snoring | 31 | | |
| Catathrenia | 7 | | |
| Long sleeper | 14 | | |

F. DETAILS REGARDING THE NETWORK ARCHITECTURE

We leveraged the DDPM++ model as implemented by Karras *et al.* [1], and modified to work on 1D timeseries in our previous work on EOG-driven sleep staging [2]. See Fig. 18 for an overview. The neural network architecture used in this work differs from [2] in two aspects. Firstly, there is an additional input between the epoch encoder and U-Net encoder in order to add the y_{m-1} of the previous output (in order to solve the ODE). Secondly, there is an additional embedding in ResNets to add the current diffusion timestep, a common practice in score-based diffusion models [1]. We will now discuss each neural network component.

A. Epoch encoder

Because the signals and the hypnograms had different sampling frequencies (128 Hz vs. 1/30 Hz), we first needed to downsample the input signal before we could use the U-Net structure of our model. To that end, we employed a context encoder, which downsampled the signals from $\mathbb{R}^{1792 \times 30 \times 128 \times 1}$ to $\mathbb{R}^{1792 \times 16}$, i.e. a context encoding of length number of epochs with 16 channels.

The context encoder worked as follows. First, a convolution of kernel size 1 expanded the number of channels from 1 to 16. Then, a series of two ResNets was employed to extract meaningful features from the input signal (see the ResNet section for further details). This pattern was repeated 5 times with 4 downsampling operations between the 5 blocks. Each downsampling operation used a kernel of [1,1,1,1] and a stride of 4, to effectively downsample the input by a factor of 4. At the end of the epoch encoder, another convolution of kernel and stride 15 was used, thus compressing the signals to a feature map of size $\mathbb{R}^{1792 \times 16}$ which was used as input to the U-Net encoder.

B. Stacking

After the epoch encoder, the feature map is concatenated channel wise with the previous estimate of the diffusion step. Following [1], we apply input scaling to the previous estimate of y_m as:

$$\tilde{y}_m = \frac{1}{\sqrt{\sigma_{data}^2 + \sigma_t^2}} \cdot y_m, \quad (1)$$

Where σ_{data} was estimated from data as $\sigma_{data} = 0.3160$ and σ_t is the current variance of the diffusion ODE. The stacking then results in an input of $\mathbb{R}^{1792 \times (16+5)} = \mathbb{R}^{1792 \times 21}$ for the U-Net encoder.

C. Note on prior networks

When we are using the network as a prior network, no input conditioning data is used. Thus, we skip the epoch encoder and the stacking operation, and we only input the previous diffused hypnogram \tilde{y}_m into the rest of the network.

D. U-Net encoder

The U-Net encoder first employed a convolution of kernel size 1 to increase the channel size from 21 to 32. Then, a Transformer layer together with two ResNet blocks was employed (see the Transformer layer section for further details). After each ResNet block, a skip connection was added to the U-Net decoder at the same resolution. This pattern of a transformer with two ResNets was repeated 4 times with 3 downsampling operations in between. Again, a kernel of [1,1,1,1] and a stride of 4 was used in the downsampling operations. The number of channels was left the same throughout the network, at a fixed 32 channels. Note that in the original DDPM++ implementation [3], an attention layer was added after each ResNet in the encoder. However, to bring down the computational complexity of our method and to make the encoder symmetric with the decoder, we employed only a single transformer layer at the start of each resolution level in the U-Net encoder.

E. Bottleneck

In the bottleneck, the feature map was of its smallest size, namely $\mathbb{R}^{28 \times 32}$. Here, one transformer layer sandwiched between two ResNet blocks was used to learn the highest-level features of the hypnogram.

F. U-Net decoder

The decoder followed a mirrored structure to the encoder. The skip connections from the corresponding resolution levels were concatenated to the inputs of each ResNet block. These connections allowed the feature maps to skip the downward path of the ‘U’ and enabled the model to learn both high-and-low level features of the hypnogram. The upsampling operation of the decoder was implemented using a transposed convolution with the same filter of [1,1,1,1].

As a final step toward creating the $y_m^{denoised}$, the U-Net decoder employed a convolution of kernel size 1 to map the input to 5 channels, where each channel corresponded to one of the five sleeps stages. A softmax activation function was then used to map each channel to a class probability. This creates a ‘hypnodensity’, a soft version of the hypnogram where each epoch is partially associated with each sleep stage according to some probability [4].

G. ResNet

The ResNet, or Residual Network, was repeated throughout the architecture. It consists of two group normalization layers and two convolutions in an alternating pattern. Group normalization, as described by [5], applies a learned normalization across groups of channels, enabling faster training. In our case, each group consisted of 4 channels. The 1D convolutions of the ResNet each used a kernel of size 7 and zero-padding set to ‘same’. Each convolution was followed by SiLU (Sigmoid Linear Unit) activation [6]. Additionally, a spatial dropout layer was added before the second convolution, which drops out entire channels during training with a probability of 10%. Spatial dropout is a better regularizer for convolutional neural networks, since neighbouring samples are often highly

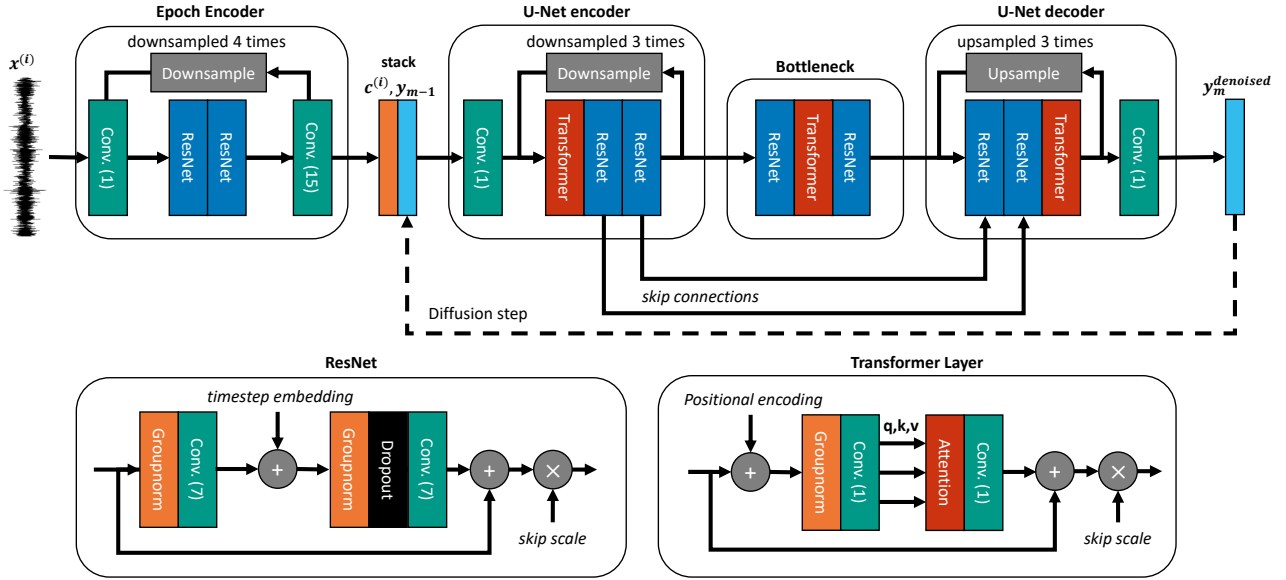


Fig. 18. Overview of the neural network used for each denoiser $D_{\theta(i)}(y_m, x^{(i)}, \sigma(t_m))$. The signal, $x^{(i)}$, is used as the initial input to the network and encoded into a context vector. This is then stacked with the sample at the current timestep y_m and fed through a U-Net structure. At the end, a hypodensity is given as output through the use of a softmax activation function. The current noise variance, $\sigma(t_m)$, is additionally embedded into a timestep embedding, which is added inside the ResNet layers of the U-Net encoder and U-Net decoder. To avoid needing to run the Epoch Encoder M times, the timestep embedding is not added to its ResNet layers.

correlated [7]. Finally, a residual connection was added to help combat vanishing gradient problems. To limit the magnitude of the signals, scaling with a factor of $skip\ scale = \sqrt{0.5}$ was applied.

In the case that the ResNet was part of the epoch encoder, the additive timestep embedding was equal to zero, and we effectively do not add it. Otherwise, an additive timestep embedding is generated from the current noise level of the diffusion process to tell it about what kind of noise level to expect in y_{m-1} , which has been found to be helpful in the score-based diffusion literature. This additive timestep embedding is explained in the sequel.

H. Timestep embedding

Following [1], the current noise level of the diffusion process, σ_t , is given as an additional input to the network in a scaled and embedded form. To that end, it is first scaled as follows:

$$\tilde{\sigma}_t = 0.25 \log(\sigma_t). \quad (2)$$

After this scaling, a sine-cosine embedding scheme was used that embedded the noise level as follows:

$$\mathbf{c} = [0, 1, \dots, C/2 - 1]^T, \quad (3)$$

$$\mathbf{f} = 1000^{-(C/2 - 1)}, \quad (4)$$

$$\mathbf{z} = [\cos(\tilde{\sigma}_t \cdot \mathbf{f}), \sin(\tilde{\sigma}_t \cdot \mathbf{f})]^T, \quad (5)$$

where C is the number of channels in the ResNet, which is equal to 32 throughout the U-Net. Subsequently, a multilayer perceptron (MLP) was applied of 2 layers, with 8 hidden nodes each and SiLU activation. Then, for each ResNet separately, a local linear layer was applied to increase the noise level embedding to 32 again. As a final step it is broadcasted into the input length of the feature map at the ResNet and added to it element-wise.

I. Transformer

The original transformer architecture is a sequence-to-sequence model composed of both an encoder and a decoder [8]. Where each element consists of a scaled dot-product attention layer and an element-wise feed-forward network. Additionally, positional encoding is added at the start of the encoding and decoding stacks. We adapt the transformer architecture to be suited for our network. Firstly, we did not use the decoder, since it is used to generate new sequence in an auto-regressive manner. Secondly, since we embedded the layers within a larger convolutional neural network, there was no need for separate element-wise feed-forward networks. lastly, because the attention layers operated at different time scales, we added positional encoding to each of them.

The positional encoding was also implemented using sine-cosine embedding. The encoding scheme used is similar to the timestep embedding, with some differences. Namely, we here create a full matrix embedding instead of only a vector embedding, no MLP is applied, and the sine and cosine terms are interleaved.

In the transformer layer positional encoding scheme, a positional encoding matrix is added element-wise to the input sequence of the transformer. To that end, the input sequence \mathbf{S} and positional encoding matrix \mathbf{P} should be of the same size: $\mathbf{S}, \mathbf{P} \in \mathbb{R}^{L \times C}$, where L is the length of the input sequence and C is the number of channels (32 in our case). The positional encoding matrix for the transformer layers is given by:

$$\begin{aligned} \mathbf{P}_{(l, 2c)} &= \sin\left(l \cdot 1000^{-2c/C}\right) \\ \mathbf{P}_{(l, 2c+1)} &= \cos\left(l \cdot 1000^{-2c/C}\right), \end{aligned} \quad (6)$$

with $l \in [0, 1, \dots, L - 1]$ and $c \in [0, 1, \dots, C/2 - 1]$. This type of encoding enables the transformer to exploit information

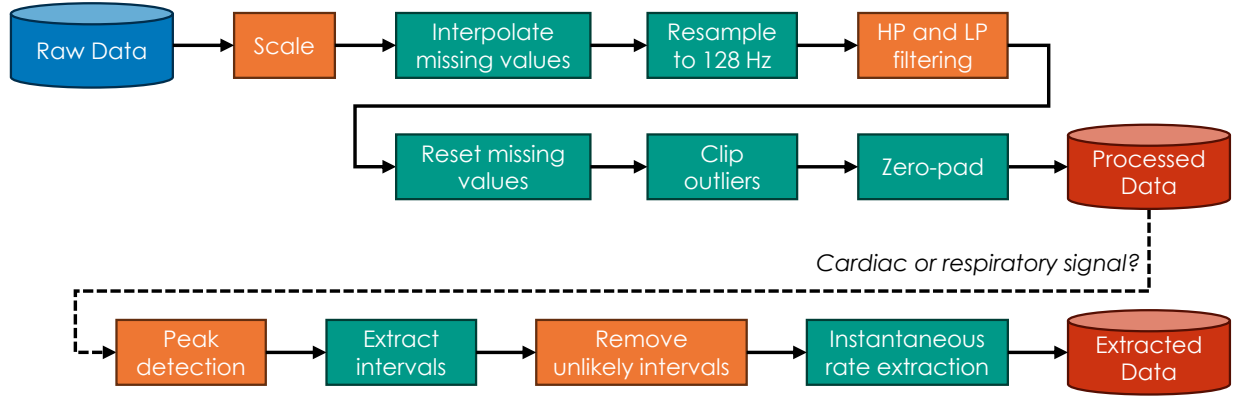


Fig. 19. The preprocessing pipeline is the same for all the signals. The orange blocks are set by signal-type specific parameters, e.g. the cutoff frequencies of the filters can be different for different signal types, see Table III. If a signal is a cardiac or respiratory signal we also extract the instantaneous heart-rate or breathing-rate.

about both the absolute and relative positions of samples along the night.

Each of the transformer layers used scaled dot-product self-attention. While the attention mechanism can be implemented using multiple attention-heads for added complexity, we here only made use of a single head. In scaled dot-product self-attention, three linear projections are applied to transform the sequence to a query, key, and value matrix:

$$\mathbf{Q} = \mathbf{S}\mathbf{W}_Q, \mathbf{K} = \mathbf{S}\mathbf{W}_K, \mathbf{V} = \mathbf{S}\mathbf{W}_V, \quad (7)$$

where $\mathbf{W}_Q, \mathbf{W}_K, \mathbf{W}_V \in \mathbb{R}^{C \times C}$ are learned linear projection weights and $\mathbf{Q}, \mathbf{K}, \mathbf{V} \in \mathbb{R}^{L \times C}$ are the query, key, and value matrices, respectively. These linear projections can be implemented efficiently by a single convolutional layer of kernel size 1 and output channel size of $3C$, as its output can be split along the channel dimension into the three separate components.

Following a database analogy, the queries are going to look for matching keys and propagate the associated values to the output, where each individual query, key, and value are found along the rows of their respective matrices. This process is defined by the scaled dot-product self-attention mechanism:

$$\text{Attention}(\mathbf{Q}, \mathbf{K}, \mathbf{V}) = \text{softmax}\left(\frac{\mathbf{Q}\mathbf{K}^T}{\sqrt{C}}\right) \mathbf{V}, \quad (8)$$

where \mathbf{K}^T denotes the transpose of the key matrix. Moreover, $\mathbf{Q}\mathbf{K}^T \in \mathbb{R}^{L \times L}$ denotes the attention map. To ensure that the magnitudes in the attention map do not grow too large, it is scaled down by a factor of $1/\sqrt{C}$. Additionally, a softmax activation is applied along the rows of the attention map in order to ensure that the attention sums to 1.

After the scaled dot-product attention layer, another linear projection using a 1D convolution was applied. Similar to the ResNet, a residual connection was applied with a scaling of $\text{skip scale} = \sqrt{0.5}$.

G. PREPROCESSING

We applied a common preprocessing pipeline to all signals as shown in Fig. 19. We will briefly describe each preprocessing operation. First, each of the signals is scaled by a constant

value in order to bring its approximate magnitude around 1. The scaling factor is chosen specific to each signal type and is shown in Table III. We for example scale all the EEG channels by a factor 10^4 , making it so that an amplitude of $100\mu\text{V}$ corresponds to the value 1 and the slow-wave amplitude threshold of $75\mu\text{V}$ corresponds to a value of 0.75 [9]. This scaling enables faster training of the neural networks.

Second, we identify missing values in the signals as those locations where they are exactly equal to 0. We linearly interpolate these values by using neighbouring sample values. This interpolation is performed in order to reduce filtering artifacts that can occur by the large jumps in magnitude that these missing values cause. After all the filtering operations, the samples with the missing values are reset to exact zeroes, this enables the neural networks to understand which values are missing in the signal.

Third, we resample all signals to 128 Hz using a polyphase filter, except for the SpO2 signal which was up-sampled from 32 Hz to 128 Hz using a sample and hold scheme. After resampling, we apply a low-pass and a high-pass filter, both implemented using fifth order butterworth filter. The high-pass and low-pass filter settings are signal type specific and reflect the recommendations of the AASM manual [9] with some minor adjustments to the low-pass filter settings.

After filtering we reset the samples values of the missing value indices back to zero. We then clip the signals between -5 and 5. For example, the EEG signals are clipped between $-500\mu\text{V}$ and $+500\mu\text{V}$. Lastly, we zero-pad all the signals to a common length of 1792 sleep epochs, or $1792 \cdot 30 \cdot 128 = 6,881,280$ samples. This zero-padding was solely done for implementation purposes, as it allows to stack the signals of different nights, and the zero-padded segment was not used to calculate any of the overnight statistics or performance metrics such as accuracy and Cohen's kappa.

In the case that the extracted signal was a cardiac or respiratory signal, such as ECG, finger PPG, or RIP Belt, we also extracted the instantaneous heart-rate (IHR) or the instantaneous breath-rate (IBR). This extraction was performed by extracting the peaks of the cardiac pulses and the breaths using the automatic multi-scale peak detection algorithm [10].

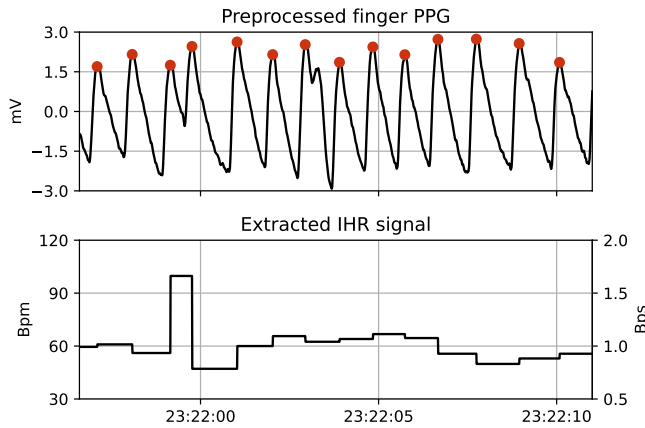


Fig. 20. Example of IHR extraction from a finger PPG signal. The red dots denote the peaks found by the automatic multi-scale peak detection algorithm.

We used the following settings: window length = 600 seconds, window overlap = 120 seconds, and maximum scale = 5 seconds for cardiac signals, while maximum scale = 60 seconds for respiratory signals. After peak detection, we convert the peaks to the inter-beat and inter-breath interval length using a sample and hold scheme. To reduce the impact of artifacts, biologically implausible intervals are removed from the sequence. We remove all cardiac inter-beat intervals outside the range of [0.3s - 2s], and we remove all respiratory inter-breath intervals outside the range of [1s - 30s]. As a final step, the intervals are converted into the IHR or IBR. While typically expressed in beats per minute (Bpm) or breaths per minute (Brpm), we scale the signals by 1/60 to get the beats/breaths per second, resulting in a better magnitude for use by the neural networks. Fig. 20 shows an example of how we extract the peaks of a finger PPG signal, which we then convert to inter-beat intervals, to subsequently convert to the IHR.

REFERENCES

- [1] T. Karras, M. Aittala, T. Aila, and S. Laine, "Elucidating the design space of diffusion-based generative models," in *Advances in Neural Information Processing Systems*, vol. 35, pp. 26565–26577, December 2022.
- [2] H. van Gorp, M. M. van Gilst, P. Fonseca, S. Overeem, and R. J. G. van Sloun, "Single-channel eeg sleep staging on a heterogeneous cohort of subjects with sleep disorders," *Physiological measurement*, pp. 1–14, 2024.
- [3] Y. Song, J. Sohl-Dickstein, D. P. Kingma, A. Kumar, S. Ermon, and B. Poole, "Score-based generative modeling through stochastic differential equations," in *International Conference on Learning Representations*, November 2021.
- [4] J. B. Stephansen *et al.*, "Neural network analysis of sleep stages enables efficient diagnosis of narcolepsy," *Nature Communications*, vol. 9, p. 5229, December 2018.
- [5] Y. Wu and K. He, "Group normalization," in *Proceedings of the European conference on computer vision (ECCV)*, pp. 3–19, 2018.
- [6] D. Hendrycks and K. Gimpel, "Gaussian error linear units (gelus)," *arXiv preprint arXiv:1606.08415*, 2016.
- [7] J. Tompson, R. Goroshin, A. Jain, Y. LeCun, and C. Bregler, "Efficient object localization using convolutional networks," in

Proceedings of the IEEE conference on computer vision and pattern recognition, pp. 648–656, 2015.

- [8] A. Vaswani *et al.*, "Attention is all you need," *Advances in neural information processing systems*, vol. 30, 2017.
- [9] C. Iber, S. Ancoli-Israel, A. Chesson, and S. F. Quan, *The AASM manual for the scoring of sleep and associated events: rules, terminology and technical specifications*. Westchester, IL, USA: American Academy of Sleep Medicine, 2007.
- [10] F. Scholkmann, J. Boss, and M. Wolf, "An efficient algorithm for automatic peak detection in noisy periodic and quasi-periodic signals," *Algorithms*, vol. 5, no. 4, pp. 588–603, 2012.